nature chemistry

ARTICLES

PUBLISHED ONLINE: 20 JULY 2009 | DOI: 10.1038/NCHEM.289

# Spin transition in a four-coordinate iron oxide

T. Kawakami[1], Y. Tsujimoto[2], H. Kageyama[2]*, Xing-Qiu Chen[3], C. L. Fu[3], C. Tassel[2], A. Kitada[2], S. Suto[4], K. Hirama[4], Y. Sekiya[4], Y. Makino[4], T. Okada[5], T. Yagi[5], N. Hayashi[6], K. Yoshimura[2], S. Nasu[7], R. Podloucky[8] and M. Takano[9]

**Spin transition has attracted the interest of researchers in various fields since the early 1930s, with thousands of examples now recognized, including those in minerals and biomolecules. However, so far the metal centres in which it has been found to occur are almost always octahedral six-coordinate $3d^4$ to $3d^7$ metals, such as Fe(II). A five-coordinate centre is only rarely seen. Here we report that under pressure $SrFe(II)O_2$, which features a four-fold square-planar coordination, exhibits a transition from high spin ($S = 2$) to intermediate spin ($S = 1$). This is accompanied by a transition from an antiferromagnetic insulating state to a ferromagnetic so-called half-metallic state: only half of the spin-down ($d_{xz}$,$d_{yz}$) states are filled. These results highlight the square-planar coordinated iron oxides as a new class of magnetic and electric materials.**

Spin transition, or spin crossover, generally occurs in compounds of octahedrally coordinated *3d* transition metal ions with $d^4$, $d^5$, $d^6$ and $d^7$ electronic configurations, and they are driven by the competition between the intra-atomic exchange energy and the crystal field energy. The former stabilizes a high-spin state, a spin state with a maximum spin multiplicity, as for the free ion, while the latter stabilizes a low-spin state in which the electrons occupy low-energy orbitals only at the expense of increasing the exchange energy[1]. These transitions, which can be induced by external perturbations, such as heat[2,3], pressure[4–8], light[9], magnetic fields[10], chemical substitution[11] and gas adsorption[12], are found in a wide range of materials, such as oxides ($FeBO_3$, $CaFeO_3$) (refs 4,5,7,10), metal–organic complexes[1], porous materials[12] and supramolecular systems[3], as well as in human haemoglobin[13]. Some of these materials have found promising applications as sensors, or as displaying and recording devices. Recent discoveries of the spin-state transition in magnesiowüstite (Mg,Fe)O (refs 4,5) and silicate perovskites $(Mg,Fe)(Si,Al)O_3$ (ref. 7) have provided further understanding of the seismic-wave heterogeneity in the Earth's lower mantle. Among the ions that exhibit spin-state transition phenomena, the largest number have been found for the $d^6$ electronic configuration, of which divalent iron(II) represents the majority. The transition has been observed mostly between the high-spin ($S = 2$) and the low-spin ($S = 0$) states.

The crystal field energy depends on the particular geometrical arrangement of both metal ion and ligands, as well as on the metal–ligand distance. It also depends on properties such as substantial deviations from octahedral symmetry, packing effects in crystal lattices, the thermal volume changes inherent to crystalline solids and cooperative interactions. For example, it is known that a transition involving an intermediate spin state ($S = 1$ for $d^6$ and $S = 3/2$ for $d^5$) is feasible for five-fold coordinated compounds, such as $TbBaCo_2O_5$, with a pyramidal coordination[14] and the $(Fe(P_4)Br)BPh_4{\cdot}CH_2Cl_2$ complex ($P_4$ = hexaphenyl-1,4,7,10-tetraphosphadecane, Ph = phenyl) with a trigonal–bypyramidal coordination[1]. To the authors' knowledge, however, up to now no spin transition has been reported for compounds with a four-coordinate (or less) metal ion.

A recently synthesized iron(II) oxide, $SrFeO_2$, as prepared by the hydride reduction of $SrFeO_3$ at low temperatures, unprecedentedly has a square-planar coordination of the high-spin iron(II) ion[15,16]. As shown in Fig. 1d, this material is built from two-dimensional $FeO_2$ layers separated by strontium atoms, isomorphic with the so-called infinite-layer structure, as first found for $(Ca,Sr)CuO_2$. In spite of an apparent two-dimensional crystal structure, it undergoes an antiferromagnetic order at a remarkably high temperature (Néel temperature, $T_N = 473$ K) into a *G*-type spin structure, which results from the strong hybridization between iron $d_{x^2-y^2}$ and oxygen $p_\sigma$ orbitals, as evidenced by a very low isomer shift in the Mössbauer spectrum.

Here we present investigations ($^{57}$Fe Mössbauer spectroscopy, electrical resistance, X-ray diffraction and first-principle calculations) on effects of pressure on the spin and electronic state in $SrFeO_2$. These showed that $SrFeO_2$ is the first material found to have a four-fold coordinated metal ion with a spin-state transition. The transition from high spin to intermediate spin is accompanied by an insulator-to-metal transition, as well as by an antiferromagnetic-to-ferromagnetic transition.

Typical high-pressure $^{57}$Fe Mössbauer spectra of $SrFeO_2$ at room temperature are shown in Fig. 2a (see Supplementary Fig. S1 for details). Below ~30 GPa, no significant change was observed within the experimental uncertainties. The hyperfine field ($H_{hf}$) at 25 GPa, for example, is 42 T, which is nearly identical with that at ambient pressure[15], and indicates that the divalent iron ion remains in the high-spin state ($S = 2$) and that $T_N$ remains high. The gradual and linear decrease in the isomer shift with pressure (see Supplementary Fig. S2) is in accordance with the trend observed in many iron compounds under high pressure[1,8], and

[1]Institute of Quantum Science, Nihon University, Chiyoda, Tokyo 101-8308, Japan, [2]Department of Chemistry, Graduate School of Science, Kyoto University, Sakyo, Kyoto 606-8502, Japan, [3]Materials Science and Technology Division, Oak Ridge National Laboratory, Oak Ridge, Tennessee 37831, USA, [4]Graduate School of Quantum Science and Technology, Nihon University, Chiyoda, Tokyo 101-8308, Japan, [5]Institute for Solid State Physics, University of Tokyo, Kashiwa, Chiba 277-8581, Japan, [6]Graduate School of Human and Environmental Studies, Kyoto University, Sakyo, Kyoto 606-8501, Japan, [7]Institute for Chemical Research, Kyoto University, Uji, Kyoto 611-0011, Japan, [8]Institute of Physical Chemistry, University of Vienna, Sensengasse 8/7, Wien, Austria, [9]Institute for Integrated Cell-Material Sciences, Kyoto University, Yoshida Ushinomita-cho, Sakyo, Kyoto 606-0801, Japan.
*e-mail: kage@kuchem.kyoto-u.ac.jp

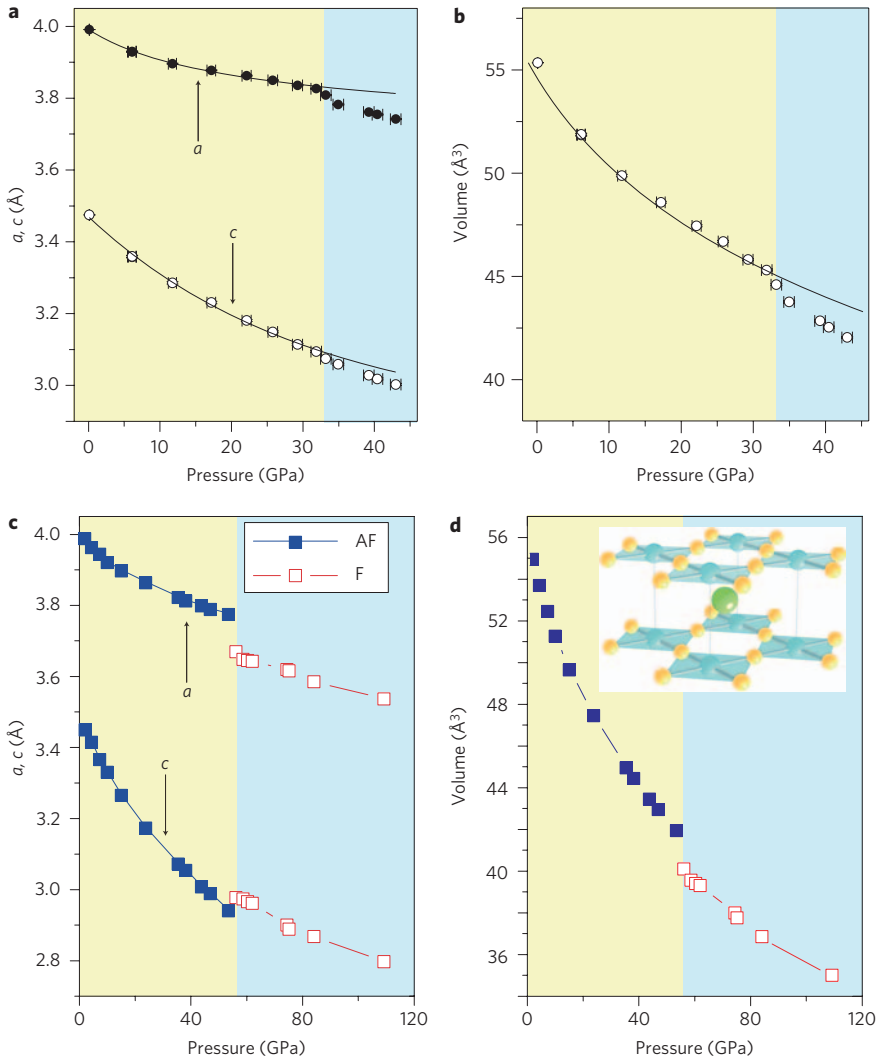


**Figure 1 | Lattice anomaly at the spin-state transition. a**,**b**, Experimental lattice parameters *a* and *c* (**a**) and the volume *V* (**b**) as a function of pressure. Standard deviations (error bars) were determined by least-squares fit, and are within the size of the symbols. The solid lines in **a** are guides to the eye and that in **b** is the fit to the third-order Birch–Murnaghan equation of state in the low-pressure phase. **c**,**d**, Calculated cell parameters and volume for the $S = 2$ antiferromagnetic (AF) state and the $S = 1$ ferromagnetic (F) state. The inset is the crystal structure of $SrFeO_2$ (**d**), in which blue, green and yellow spheres represent iron, strontium and oxygen atoms, respectively.

can be interpreted in terms of a gradually increased hybridization of iron 3*d* orbitals with the 2*p* orbitals of the oxygen neighbours.

A drastic change, however, arose in the Mössbauer spectrum at a pressure of 38 GPa. Although it also consists of six well-defined peaks, which indicates the presence of magnetic order at ambient temperature, the field $H_{hf} = 18$ T is only about half of that for the low-pressure phase, which implies the occurrence of a spin-state transition into an intermediate spin ($S = 1$) state. This spectral feature remains up to the maximum pressure of 70 GPa applied in this study. To confirm the spin-state transition, in other words to exclude the possibility that the reduction in $H_{hf}$ is merely a result of the reduction in $T_N$, we cooled the sample to 7 K. The corresponding spectrum has an only slightly increased $H_{hf}$ value of 19 T, which provides firm evidence that the iron ions in the high-pressure phase are in the intermediate spin state. The well-developed six-line pattern in the intermediate spin state indicates that the magnetic-order temperature is still far above room temperature. Subsequently, Mössbauer spectroscopy of the high-pressure phase was conducted under a magnetic field, for which the incident γ-ray was set parallel to the applied magnetic field. As shown in Fig. 2 and Supplementary Fig. S3, the intensities of the second and fifth lines ($\Delta m = 0$) showed a remarkable decrease with increasing magnetic field and disappeared at 3 T. We thus conclude that the high-pressure phase is ferromagnetic. The quadrupole shift ($QS = s_1 - s_2$) changed suddenly from 1.53 mm s$^{-1}$ (25 GPa) to 0.70 mm s$^{-1}$ (38 GPa) after the transition. Both the initial and the new spectra coexist in the pressure range 27–37 GPa because of a pressure gradient within the sample. However, analysis of the relative spectrum weight and the pressure gradient gave a rough estimate of the critical pressure $P_c$ as $33 \pm 3$ GPa.

To examine the possibility of structural change on the spin transition, we carried out *in situ* X-ray powder diffraction experiments in a diamond anvil cell at pressures up to 43 GPa. The diffraction data recorded (see Supplementary Fig. S4) are of high quality with a good signal-to-noise ratio, and so allowed an accurate determination of the lattice parameters. All the peaks of the diffraction pattern at each pressure could be assigned to a tetragonal infinite-layer structure, and no additional reflections were detected within the resolution of the experiment. Although the measured range of the diffraction angles is not sufficient to confirm this fully, it is likely that the transition is isostructural. At pressures below the spin transition, the pressure dependence of the volume can be fitted by the third-order

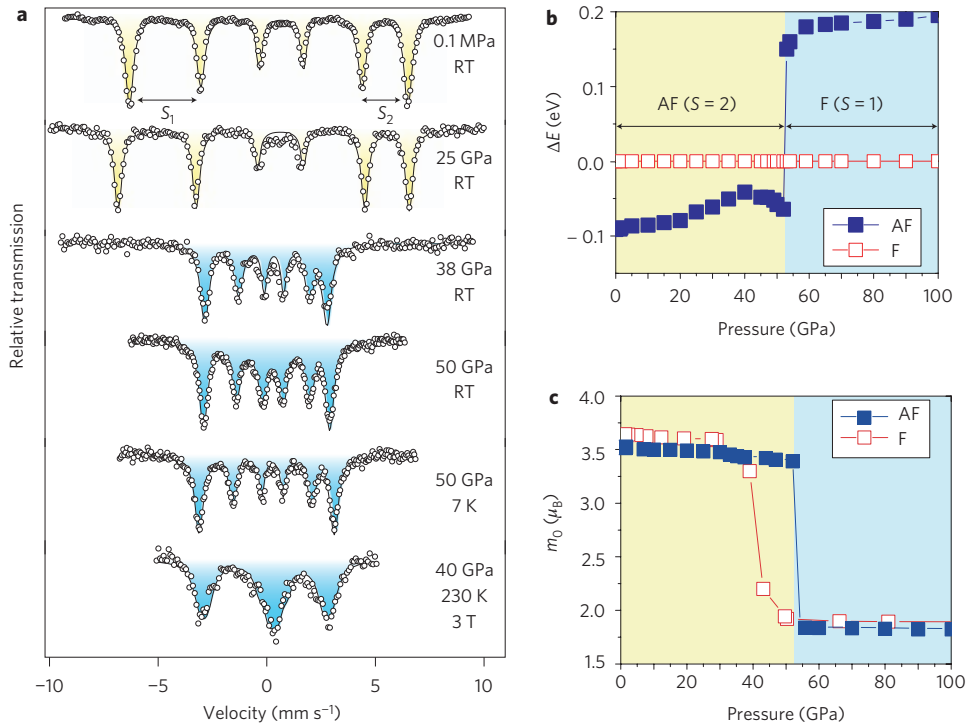


**Figure 2 | Transition from high spin to intermediate spin in $SrFeO_2$ under high pressure. a**, Typical high-pressure $^{57}$Fe Mössbauer spectra obtained from $SrFeO_2$ (see Supplementary Fig. 1 for detail). The yellow spectra correspond to the $S=2$ state, and the blue to the $S=1$ state. The solid lines represent the fitted curves. $S_1$ and $S_2$ correspond, respectively, to the split between the first and second peaks and that between the fifth and sixth peaks. Velocity scale is relative to α-Fe at room temperature (RT). **b**, Calculated energy difference ($\Delta E$) between the $S=2$ antiferromagnetic (AF) state and the $S=1$ ferromagnetic (F) state. **c**, Calculated spin moment ($m_0$) for the $S=2$ antiferromagnetic (AF) state and the $S=1$ ferromagnetic (F) state.

Birch–Murnaghan equation of state with the bulk modulus $K=$ 126 GPa, which is slightly smaller than that estimated for the fully oxidized perovskite $SrFeO_3$ ($K=146$ GPa) (ref. 17). As displayed in Fig. 1a, the unit cell parameters $a$ and $c$ decrease smoothly with the application of pressure, but exhibit a significant drop at $33\pm1$ GPa, which agrees well with $P_c$ as estimated from the Mössbauer study. Therefore, this anomaly might be associated with the claimed spin transition. A volume reduction of ~3% (Fig. 1b) is comparable with those for other compounds that exhibit high-spin to low-spin transitions[1].

First-principle calculations based on the hybrid density functional theory (PBE0) method[18,19] were carried out to examine the pressure dependence of the crystal and electronic structures. The antiferromagnetic $S=2$ state is the ground state at atmospheric pressure and remains stable up to $P_c$, where the abrupt transition to the ferromagnetic $S=1$ state occurs (Fig. 2b), in accordance with the experimental observations. The calculated $P_c$ of 53 GPa (see also Fig. 1c,d) is, however, rather high in comparison with the experimental $P_c$ of 33 GPa. As shown in Fig. 2c, the calculated spin moment decreases from $3.5\mu_B$ to $1.8\mu_B$ between the antiferromagnetic and ferromagnetic states, which is consistent with the change in $H_{hf}$ from 42 T to 19 T. With respect to the $a$ axis, both theory and experiment indicated a drop of ~2%, but for the $c$ axis the changes given by theory and experiment did not correlate. However, in terms of the unit-cell volume at $P_c$, the discrepancy between theory and experiment is only ~3 Å$^3$ (or 6%).

To understand the nature of the spin transition, we first focused on the antiferromagnetic $S=2$ state. The local density of states (DOS) of the iron ion at atmospheric pressure is shown in Fig. 3a. Consistent with the results of previous 'LDA + U' calculations[20,21], the lone spin-down electron was found to occupy the $d_{z^2}$ orbital. The double occupation of $d_{z^2}$ allows a considerable reduction of the intra-atomic Coulomb repulsion[20,21]. The $\sigma$-bond formed between iron $d_{x^2-y^2}$ and oxygen $p_{x,y}$ is split into the bonding and antibonding states by ~7 eV owing to a strong in-layer iron $d$ and oxygen $p$ hybridization. For pressures less than $P_c$, both the bonding and antibonding states in the spin-up channel are occupied. In the antiferromagnetic $S=2$ state, the $d^6$ state has the electronic configuration of $(d_{z^2})^2(d_{xz},d_{yz})^2(d_{xy})^1(d_{x^2-y^2})^1$.

We attribute the spin transition to the strong in-layer hybridization between iron $d_{x^2-y^2}$ and oxygen $p_\sigma$ bonding states, which leads to electronic instability towards the depopulation of $d_{x^2-y^2}$ and oxygen $p_\sigma$ antibonding states. Figure 3b shows the local iron DOS for the ferromagnetic $S=1$ state, which demonstrates the depopulation of the iron $d_{x^2-y^2}$ antibonding states. The iron $d$ electrons are increased to $d^{6.5}$ in total, with the electronic configuration of $(d_{z^2})^1(d_{xz},d_{yz})^2(d_{xy})^1(d_{x^2-y^2})^{0.25}$ for the spin-up channel and $(d_{z^2})^1(d_{xz},d_{yz})^1(d_{xy})^0(d_{x^2-y^2})^{0.25}$ for the spin-down channel. Another point is that the ferromagnetic $S=1$ state is half metallic. In the antiferromagnetic $S=2$ state, the bandgap decreases considerably with increasing pressure, as shown in Fig. 4a, and then drops to zero at $P_c$.

The spin moment of the iron $d_{x^2-y^2}$ bonding states is quenched because of the enhanced in-layer bonding between iron $d$ and oxygen $p$. The double occupation of $d_{z^2}$ is maintained in the ferromagnetic $S=1$ state just after the transition, but becomes energetically unfavourable because of the compression of the interlayer spacing. Therefore, a charge transfer from spin-down $d_{z^2}$ to spin-down $d_{xy}$ has to occur, whereas the spin-down $(d_{xz},d_{yz})$ states remain half-occupied (Fig. 3c). It follows that, as the pressure reaches ≥70 GPa, the spin-down states of $d_{xy}$ and $d_{z^2}$ also become half-occupied in the ferromagnetic $S=1$ state $(d_{z^2})^{0.5}(d_{xz},d_{yz})^1(d_{xy})^{0.5}$ $(d_{x^2-y^2})^{0.25}$ for the spin-down states, which results in an increase of the DOS at the Fermi level.

We conducted electrical resistance measurements on non-sintered powder samples under pressure, as summarized in Fig. 4.

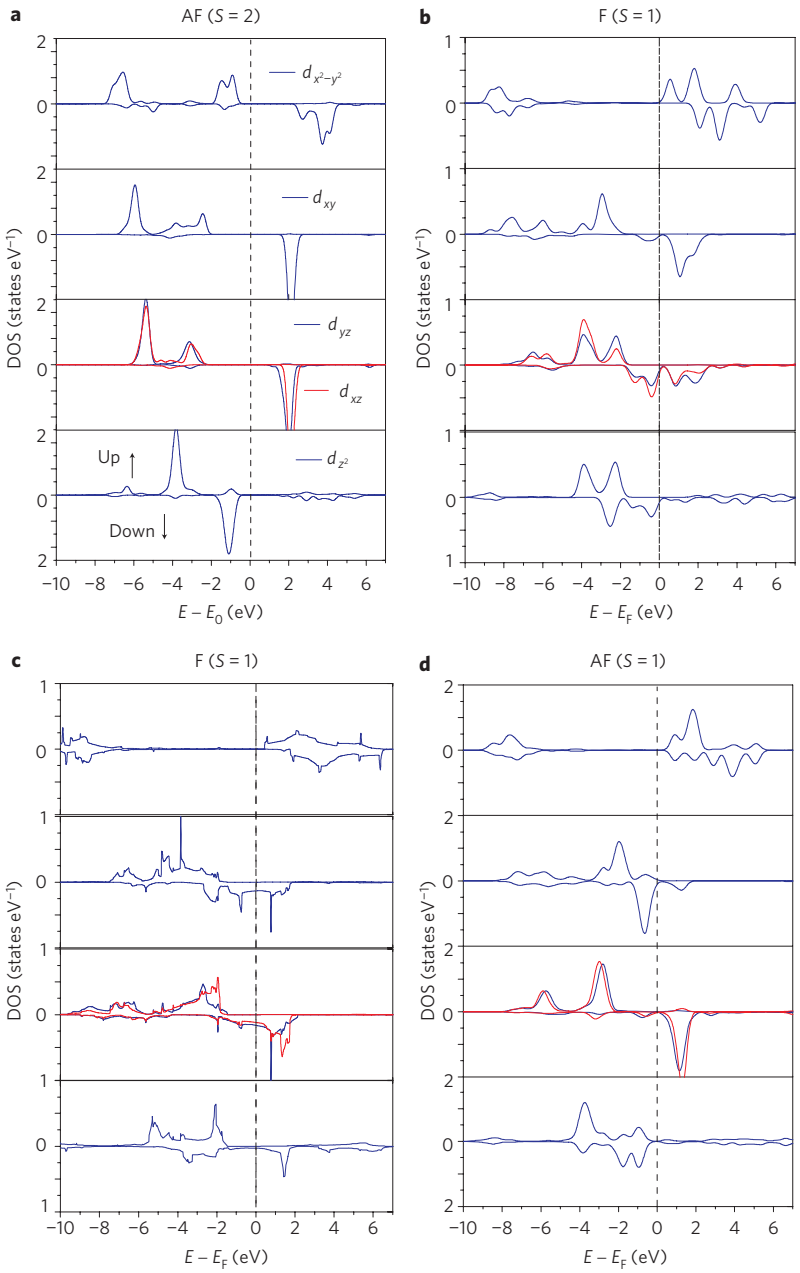


**Figure 3 | Calculated local density of states of iron in $SrFeO_2$. a**, High-spin ($S = 2$) antiferromagnetic (AF) state at 0 GPa (insulating). **b**, Intermediate-spin ($S = 1$) ferromagnetic (F) state at 53 GPa (metallic). **c**, Intermediate-spin ($S = 1$) ferromagnetic (F) state at 70 GPa (metallic). **d**, Unstable intermediate-spin ($S = 1$) antiferromagnetic (AF) state at 65 GPa. In the $S = 2$ antiferromagnetic state (**a**), the lone spin-down electron occupies the spin-down $d_{z^2}$ orbital. In the $S = 1$ ferromagnetic state (**b**), the $d_{x^2-y^2}$ antibonding states become unoccupied, which results in the charge transfer from $d_{x^2-y^2}$ to $d_{yz}$ (or $d_{xz}$). The $d_{z^2}$ orbital maintains its double occupation through the spin-state transition at 53 GPa. The energy zero is set at the middle of the gap (**a**) and at the Fermi level (**b**,**c**,**d**).

At ambient and low pressures, $SrFeO_2$ is a non-conductor or a semiconductor with an out-of-range resistance. The electrical resistance at room temperature became measurable above 17 GPa. Across the spin-state transition, a drastic decrease of resistance occurred from kiloohms at 27 GPa to ohms at 37 GPa, and to centiohms at 50 GPa. The temperature dependence of the electrical resistance $\Delta R/\Delta T$ became smaller and, finally, its sign changed from negative to positive at ~60 GPa. Although $\Delta R/\Delta T$ turns negative at lower temperatures, this possibly results from Anderson localization and the use of the non-sintered powder sample. In addition, the resistance measurements suffered from the pressure distribution within the sample, as in the Mössbauer experiments, which must, to some extent, obscure the insulator–metal transition at $P_c$. It is likely that the intermediate spin state is metallic, as theoretically suggested.

Compared with the ferromagnetic $S = 1$ state, the antiferromagnetic $S = 1$ state is much less stable above $P_c$. An examination of the electronic structure of its antiferromagnetic $S = 1$ state (Fig. 3d) shows that, in addition to having a $d_{z^2}$ electron in the spin-down channel, the second spin-down electron actually prefers to occupy the $d_{xy}$ orbital. The sudden increase in the energy from antiferromagnetic $S = 2$ to antiferromagnetic $S = 1$ results from the increase of Coulomb repulsion caused by the double occupation of $d_{xy}$. We have also examined the possibility of spin transition induced by

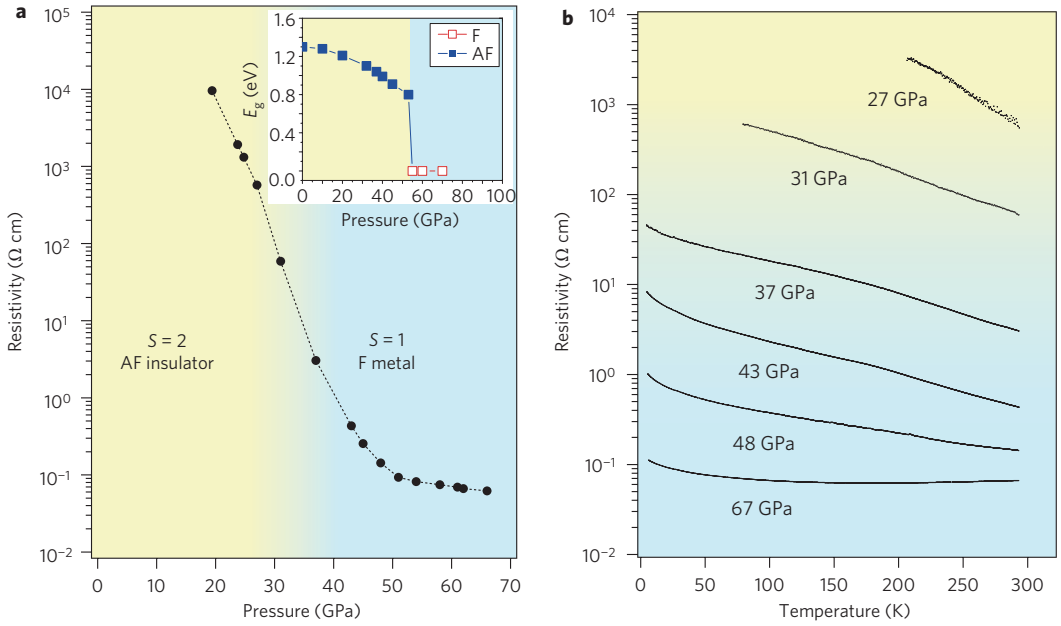


**Figure 4 | Insulator–metal transition at the spin transition. a**, Room-temperature electrical resistivity of $SrFeO_2$, which shows an insulating state for the low-pressure phase ($P < P_c$) and a metallic state for the high-pressure phase ($P > P_c$). The inset represents the calculated energy gap for the $S = 2$ antiferromagnetic (AF) state and the $S = 1$ ferromagnetic (F) state, consistent with the experimental results. **b**, Temperature dependence of the electrical resistivity under pressure.

phonon instability at various pressures. More specifically, we considered the effects of Jahn–Teller lattice distortion and breathing phonon mode. The former could induce a spin state of $S = 1$, whereas the latter could result in a coexistence of the $S = 1$ and $S = 2$ states through a charge-disproportionation reaction. However, we found experimentally and theoretically that $SrFeO_2$ is stable against a cooperative oxygen displacement in either Jahn–Teller lattice distortion or breathing phonon mode in both antiferromagnetic and ferromagnetic states at all pressures. Therefore, the spin transition in $SrFeO_2$ is not caused by these phonon instabilities.

The spin-state transitions in 3*d* ions are routinely interpreted as a result of the transfer of one or two electrons between *d* orbitals of opposite spin channels. The observed $S = 2$ to $S = 1$ transition in $SrFeO_2$ is distinctly different from previously reported examples in two aspects: it involves the transfer of non-integer *d* electrons and the $p \rightarrow d$ charge transfer (see Supplementary Table 1).

A number of transition-metal oxides[22–26] have been found to exhibit half-metallic ferromagnetism – these are limited mostly to manganese and chromium oxides ($La_{1.3}Sr_{0.7}Mn_2O_7$, $Tl_2Mn_2O_7$, $CrO_2$, and so on.). The double-perovskite oxide $Sr_2FeMoO_6$ is known as an iron-based half-metallic ferromagnet, but it contains molybdenum, which is rare in the Earth's crust. As iron is the most abundant transition metal, the discovery of half-metallic ferromagnetism in $SrFeO_2$ containing only iron is important for future applications in industry related to magnetism and spin electronics, although $P_c$ is still too high. Recent studies[27–29] demonstrated that the square-planar coordination around iron in $SrFeO_2$ is not a mere fortuity, but could be widely and universally available, and include serial spin-ladders $Sr_{n+1}Fe_nO_{2n+1}$, such as $Sr_3Fe_2O_5$ ($n = 2$). Also, a square-planar $FeO_4$ unit can be distorted towards a tetrahedron, as in $CaFeO_2$. Although $P_c$ in $SrFeO_2$ is too high, it is desirable to reduce $P_c$ in those related iron oxides and yet keep the transition temperature far above room temperature.

Metallization of the $FeO_2$ sheet would provide a hope that increased pressure could lead to superconductivity, in analogy with the layered cuprates. It is also interesting to compare the present compound with the recently discovered iron oxypnictide superconductors[30], because in both cases the iron atoms form two-dimensional square lattices and are coordinated by four anions. Furthermore, preliminary calculations at higher pressures suggest a transition from the $S = 1$ spin state to a second intermediate spin state ($S = 1/2$) before it finally falls into the $S = 0$ spin state. It would be interesting to check these points experimentally.

## Methods

The powder sample of $SrFeO_2$ was synthesized by the reaction with $CaH_2$ of a slightly oxygen-deficient perovskite, $SrFeO_{2.875}$. The precursor $SrFeO_{2.875}$ was prepared by a high-temperature ceramic method from $SrCO_3$ (99.99%) and $Fe_2O_3$ (99.99%). $SrFeO_{2.875}$ and a 2 M excess of $CaH_2$ were mixed, finely ground in an argon-filled dry box, sealed in an evacuated Pyrex tube and left to react at 553 K for two days. The residual $CaH_2$ and the CaO by-product were removed from $SrFeO_2$ by washing them out with a $NH_4Cl$–methanol solution. For details, refer to the literature[15].

The high-pressure $^{57}Fe$ Mössbauer measurements were performed up to 70 GPa using a Bassett-type diamond-anvil cell[31]. The $^{57}Fe$-enriched $SrFeO_2$ powder and small ruby chips were enclosed in the hole of a rhenium gasket. Two types of pressure-transmitting media, a 4:1 methanol:ethanol solution and Daphne7373, were used. A point $\gamma$-ray source of $^{57}Co$ in a rhodium matrix of 370 MBq and another one of 925 MBq with active areas of 1 mm and 4 mm in diameter, respectively, were used. The pressure was determined by means of ruby-fluorescence manometry. To estimate the pressure distribution along the sample, several ruby chips were placed inside the hole at different distances from its centre. It was found that the pressure gradient at the sample was not more than 8 GPa at maximal pressures. The $\gamma$-ray source could not be narrowed more because the high-pressure Mössbauer study allowed only a limited sample, and a long exposure time, as long as a week, was required to accumulate fairly reasonable spectral statistics. The magnetic field was produced by a superconducting solenoid operated in the persistent mode up to 3 T. $^{57}Fe$ Mössbauer experiments under the external magnetic field were carried out with the magnetic field applied along the $\gamma$-ray propagation direction. The velocity scale of the spectrum was relative to $\alpha$-Fe at room temperature. Electrical resistance was measured with a standard d.c. four-probe method between 5 K and 300 K up to 67 GPa. Fine alumina powder and NaCl were pressed onto the gasket surface to give electrical insulation and a pressure-transmitting medium, respectively, on which sample powder and platinum electrodes were placed together. Applied pressure was measured by means of fluorescence manometer on ruby chips placed around the sample. In this electrical resistance measurement, the initial sectional area and the distance between probes were about 60 μm × 50 μm and 50 μm, respectively.

Powder X-ray diffraction profiles at high pressures up to 43 GPa were recorded using Mo-*K*α radiation from a 5.4 kW Rigaku rotating anode generator equipped

with a 100 μm collimator. A powder sample of $SrFeO_2$ was loaded into a 300 μm hole of a pre-indented stainless-steel gasket of the diamond-anvil cell. A 4:1 methanol:ethanol mixture was used as the pressure-transmitting medium. The shift of ruby fluorescence was used to determine the pressure. To estimate the pressure distribution along the sample, several ruby chips were placed inside the hole at different distances from its centre. It was found that the pressure gradient at the sample was not more than 0.5 GPa at maximal pressures. The diffracted X-rays were collected with an image plate. More details of the experimental setup are reported elsewhere[32]. Four diffraction peaks, 110, 011, 020 and 121, were used to calculate the cell parameters.

The first-principle calculations were performed using the Vienna *ab initio* Simulation Package (VASP)[33] with the ion–electron interaction described by the projector-augmented wave potential (PAW)[34] (see Supplementary Information for details). We employed the hybrid density functional theory (PBE0) method[18,35], as implemented in VASP[19,36], to treat the localized $Fe^{2+}$ states in $SrFeO_2$. The exchange energy in PBE0 mixes the energies of exact Hartree–Fock (HF) exchange and PBE exchange from the local density functional approximation[19,36]. The long-range part of the HF-exchange interaction is included in PBE0. The weight of HF exchange in the mixing was generally less than 25%. We found that weights between 10 and 20% HF exchange provided the most consistent results and described the experimental findings reasonably well for $SrFeO_2$. The results reported in this paper were obtained using 15% HF with 85% PBE for the exchange energy. We found that the spin-transition pressure from the antiferromagnetic ($S = 2$) state to the ferromagnetic state is insensitive to the weights of mixing. It is the stable ranges of the $S = 2$ and $S = 1$ states within the ferromagnetic ordering that show an increased sensitivity to the weights of HF mixing in PBE0.

In our calculations, the semicore states (the 3*p* and 4*s* states of strontium and the 3*p* state of iron) were treated as valence states. An energy cutoff of 500 eV was chosen for the plane-wave expansion. Full relaxation of atomic positions and lattice parameters at each pressure was achieved by minimizing the forces and stress-tensor components. Forces were minimized down to $10^{-5}$ eV $Å^{-1}$ and the difference in the total energies between two successive electronic iterations was required to be less than $10^{-7}$ eV. The angular momentum projected local density of states and magnetic moments of iron were calculated within a sphere of 1.164 Å.

Received 9 April 2009; accepted 10 June 2009; published online 20 July 2009

## References


1. Gütlich, P. & Goodwin, H. A. *Spin Crossover in Transition Metal Compounds I–III*, Vols 233–235 (Springer, 2004).
2. Kröber, J., Codjovi, E., Kahn, O., Croliére, F. & Jay, C. A spin transition system with a thermal hysteresis at room temperature. *J. Am. Chem. Soc.* **115,** 9810–9811 (1993).
3. Real, J. A. *et al.* Spin crossover in a catenane supramolecular system. *Science* **267,** 265–267 (1995).
4. Badro, J. *et al.* Iron partitioning in earth's mantle: toward a deep lower mantle discontinuity. *Science* **300,** 789–791 (2003).
5. Lin, J.-F. *et al.* Spin transition of iron in magnesiowüstite in the earth's lower mantle. *Nature* **436,** 377–380 (2005).
6. Rueff, J.-P. *et al.* Pressure-induced high-spin to low-spin transition in FeS evidenced by X-ray emission spectroscopy. *Phys. Rev. Lett.* **82,** 3284–3287 (1999).
7. Li, J. *et al.* Electronic spin state of iron in lower mantle perovskite. *Proc. Natl Acad. Sci. USA* **101,** 14027–14030 (2004).
8. Takano, M. *et al.* Pressure-induced high-spin to low-spin transition in $CaFeO_3$. *Phys. Rev. Lett.* **67,** 3267–3270 (1991).
9. Decurtins, S., Gütlich, P., Köhler, C. P., Spiering, H. & Hauser, A. Light-induced excited spin state trapping in a transition-metal complex: the hexa-1-propyltetrazole-iron (II) tetrafluoroborate spin-crossover system. *Chem. Phys. Lett.* **105,** 1–4 (1984).
10. Qi, Y., Müller, E. W., Spiering, H. & Gütlich, P. The effect of a magnetic field on the high-spin ↔ low-spin transition in $[Fe(phen)_2(NCS)_2]$. *Chem. Phys. Lett.* **101,** 505–505 (1983).
11. Ikeue, T. *et al.* Saddle-shaped six-coordinate iron(III) porphyrin complexes showing a novel spin crossover between $S = 1/2$ and $S = 3/2$ spin state. *Angew. Chem. Int. Ed.* **40,** 2617–2620 (2001).
12. Halder, G. J., Kepert, C. J., Moubaraki, B., Murray, K. S. & Cashion, J. D. Guest-dependent spin crossover in a nanoporous molecular framework material. *Science* **298,** 1762–1765 (2002).
13. Nakano, N., Nakano, K. & Tasaki, A. A magnetic study of acidic ferric hemoglobin. *Biochem. Biophys. Acta* **251,** 301–313 (1971).
14. Moritomo, Y. *et al.* Metal–insulator transition induced by a spin-state transition in $TbBaCo_2O_{5+\delta}$ ($\delta = 0.5$). *Phys. Rev. B.* **61,** R13325–R13328 (2000).
15. Tsujimoto, Y. *et al.* Infinite-layer iron oxide with a square-planar coordination. *Nature* **450,** 1062–1065 (2007).
16. Köhler, J. Square-planar coordinated iron in the layered oxoferrate(II) $SrFeO_2$. *Angew. Chem. Int. Ed.* **47,** 4470–4472 (2008).
17. Kawakami, T. *et al.* High-pressure Mössbauer and X-ray powder diffraction studies of $SrFeO_3$. *J. Phys. Soc. Jpn* **72,** 33–36 (2003).
18. Perdew, M., Ernzerhof, M. & Bruke, A. Rationale for mixing exact exchange with density functional approximations. *J. Chem. Phys.* **105,** 9982–9985 (1996).
19. Paier, J. *et al.* Screened hybrid density functionals applied to solids. *J. Chem. Phys.* **124,** 154709 (2006).
20. Xiang, H. J., Wei, S.-H. & Whangbo, M.-H. Origin of the structural and magnetic anomalies of the layered compound $SrFeO_2$: a density functional investigation. *Phys. Rev. Lett.* **100,** 167207 (2008).
21. Pruneda, J. M., Inigquez, J., Canadell, E., Kageyama, H. & Takano, M. Understanding the unique structural and electronic properties of $SrFeO_2$. *Phys. Rev. B* **78,** 115101 (2008).
22. Hwang, H. Y. & Cheong, S.-W. Enhanced intergrain tunneling magnetoresistance in half-metallic $CrO_2$ films. *Science* **278,** 1607–1609 (1997).
23. Kimura, T. *et al.* Interplane tunneling magnetoresistance in a layered manganite crystal. *Science* **274,** 1698–1701 (1996).
24. Okimoto, Y. *et al.* Anomalous variation of optical spectra with spin polarization in double-exchange ferromagnet: $La_{1-x}Sr_xMnO_3$. *Phys. Rev. Lett.* **75,** 109–112 (1995).
25. Shimakawa, Y., Kubo, Y. & Manako, T. Giant magnetoresistance in $Tl_2Mn_2O_7$ with the pyrochlore structure. *Nature* **379,** 53–55 (1996).
26. Park, J.-H. *et al.* Direct evidence for a half-metallic ferromagnet. *Nature* **794,** 794–796 (1998).
27. Kageyama, H. *et al.* Spin-ladder iron oxide $Sr_3Fe_2O_5$. *Angew. Chem. Int. Ed.* **47,** 5740–5745 (2008).
28. Tassel, C. *et al.* Stability of the infinite layer structure with iron square planar coordination. *J. Am. Chem. Soc.* **130,** 3764–3765 (2008).
29. Tassel, C. *et al.* $CaFeO_2$: a new type of layered structure with iron in a distorted square planar coordination. *J. Am. Chem. Soc.* **130,** 214410–214419 (2008).
30. Kamihara, Y., Watanabe, T., Hirano, M. & Hosono, H. Iron-based layered superconductor $La[O_{1-x}F_x]FeAs$ ($x = 0.05$–$0.12$) with $T_c = 26$ K. *J. Am. Chem. Soc.* **130,** 3296–3297 (2008).
31. Bassett, W. A., Takahashi, T. & Stook, P. W. X-ray diffraction and optical observations on crystalline solids up to 300 kbar. *Rev. Sci. Instrum.* **38,** 37–42 (1967).
32. Arora, A. K., Yagi, T., Miyajima, N. & Mary, T. A. Amorphization and decomposition of scandium molybdate at high pressure. *J. Appl. Phys.* **97,** 013508 (2005).
33. Kresse, G. & Furthmuller, J. Efficiency of *ab-initio* total energy calculations for metals and semiconductors using a plane-wave basis set. *Comput. Mater. Sci.* **6,** 15–50 (1996).
34. Kresse, G. & Joubert, D. From ultrasoft pseudopotentials to the projector augmented-wave method. *Phys. Rev. B* **59,** 1758–1775 (1999).
35. Perdew, J. P., Burke, K. & Ernzerhof, M. Generalized gradient approximation made simple. *Phys. Rev. Lett.* **77,** 3865–3868 (1996).
36. Paier, J., Hirschl, R., Marsman, M. & Kresse, G. The Perdew–Burke–Ernzerhof exchange-correlation functional applied to the G2-1 test set using a plane-wave basis set. *J. Chem. Phys.* **122,** 234102 (2005).


## Acknowledgements

This work was supported by Science Research on Priority Areas (Novel States of Matter Induced by Frustration) and also partly by the Ministry of Education, Culture, Sports, Science and Technology of Japan. Research at Oak Ridge National Laboratory was sponsored by the Division of Materials Sciences and Engineering, US Department of Energy, under contract with UT-Battelle. This research used resources of the National Energy Research Computing Center, which is supported by the Office of Science of the US Department of Energy. This work was supported by the University of Vienna through the University Focus Research Area Materials Science (Multi-scale Simulations of Materials Properties and Processes in Materials).

## Author contributions

H.K. designed and coordinated the overall study seeking advice from M.T. (experiment) and C.L.F. (theory). N.H. conceived the high-pressure Mössbauer study, and X-Q.C. conceived the theoretical studies. Y.T., with support from K.Y., synthesized the material. T.K., S.S., K.H., Y.S. and Y.M. conducted high-pressure Mössbauer and electrical resistivity experiments, and T.K. analysed the data (with the help of M.T. and S.N.). Y.T., C.T., A.K., T.O. and T.Y. performed high-pressure X-ray diffraction experiments, and Y.T. and C.T. analysed the data. X-Q.C., C.L.F. and R.P. performed the theoretical work and analysis. H.K. and T.K. co-wrote the experimental part and C.L.F. and X-Q.C. co-wrote the theoretical part, with comments from R.P. All contributed to the discussion of the results.

## Additional information

Supplementary information accompanies this paper at www.nature.com/naturechemistry. Reprints and permission information is available online at http://npg.nature.com/reprintsandpermissions/. Correspondence and requests for materials should be addressed to H.K.